



ChemComm

**Optimizing Electron Transfer from CdSe QDs to  
Hydrogenase for Photocatalytic H<sub>2</sub> Production**

Journal:	<i>ChemComm</i>
Manuscript ID	CC-COM-02-2019-001150.R1
Article Type:	Communication

SCHOLARONE™  
Manuscripts

## Optimizing Electron Transfer from CdSe QDs to Hydrogenase for Photocatalytic H<sub>2</sub> Production

Monica L. K. Sanchez,<sup>a</sup> Chang-Hao Wu,<sup>b</sup> Michael W. W. Adams,<sup>b</sup> R. Brian Dyer<sup>\*a</sup>

Received 00th January 20xx,  
Accepted 00th January 20xx

DOI: 10.1039/x0xx00000x

www.rsc.org/

**A series of viologen related redox mediators of varying reduction potential has been characterized and their utility as electron shuttles between CdSe quantum dots and hydrogenase enzyme has been demonstrated. Tuning the mediator LUMO energy optimizes performance of this hybrid photocatalytic system by balancing electron transfer rates of the shuttle.**

Artificial photosynthetic systems usually employ separate modules to accomplish the essential functions of efficient light harvesting, charge separation and catalytic proton coupled electron transfer (PCET) reactions to make high energy chemical bonds.<sup>1-3</sup> This approach mimics natural photosynthetic systems and allows for the independent optimization of each module for its specific task. Hybrid quantum-dot/enzyme photocatalysts are promising examples of this modular approach.<sup>3-5</sup> The nanocrystalline semiconductor (NCS) material acts as both the light harvesting and charge separation module. It can be designed to generate long-lived reductive or oxidative equivalents with high quantum efficiency. Enzymes that catalyze PCET reactions operate with little overpotential at rates that match or exceed the rate of generation of redox equivalents by the solar flux.<sup>6</sup> Thermophilic enzymes have high stability and durability, yielding high turnover numbers (TON).<sup>7</sup> Even when these modules have been highly optimized, however, the difficult challenge that remains is how to transfer reactive electrons between modules. Both natural and artificial systems have employed redox mediators, small molecule electron carriers capable of moving between modules and efficient redox cycling. The challenges with this approach include generating sufficient driving force for multiple electron transfer (ET) steps, efficient interfacial ET and avoiding back ET.<sup>8</sup> Methyl viologen (MV) and closely related molecules have been widely employed as

electron relays largely because of their stable, long-lived radicals, commercial availability and solubility in water.<sup>9-12</sup> Most studies aimed at optimizing ET to and from the mediator have focused on manipulating the light harvesting/charge separation material.<sup>9, 10</sup> Not as much attention has been given to tuning the mediator structure and redox potential for improving ET efficiency.<sup>8, 12, 13</sup> Here, we have investigated the effects of mediator structure and reduction potential on the overall efficiency of a hybrid CdSe quantum-dot/mediator/[NiFe]-hydrogenase photocatalytic system. We varied the structure of viologen-like mediators by introducing methyl substituents and a carbon chain linking the two pyridyl nitrogens, as shown in Fig. 1. These modifications expand the range of reduction potentials of the mediators. We characterized this series of mediators structurally, spectroscopically and electrochemically and determined the effects of these mediator properties on photocatalytic production of hydrogen in the hybrid QD/hydrogenase system.

The mediator structure influences its performance as an

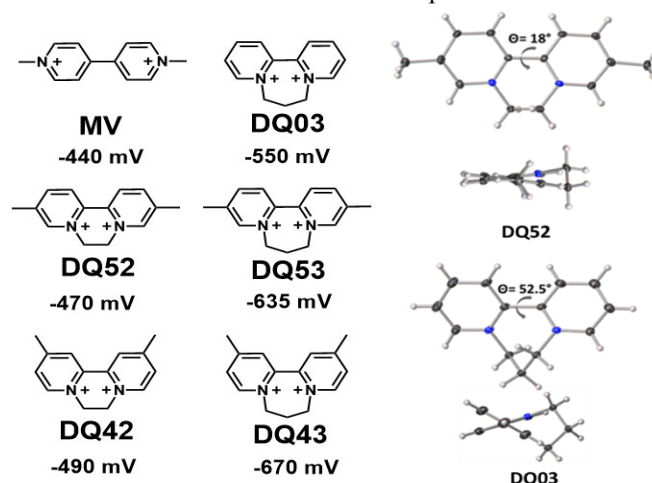


**Fig. 1** Viologen-like molecules utilized as electron shuttles, along with electrochemically determined reduction potentials (vs. NHE). The numbering scheme refers to the position of the methyl substituents (4 or 5) and the length of the carbon chain (2 or 3). The X-ray structures (right) of DQ52 and DQ03 show how the twist angle depends on the carbon-linker chain length.

<sup>a</sup> Department of Chemistry, Emory University, Atlanta, GA 30322 USA.

<sup>b</sup> Department of Biochemistry and Molecular Biology, University of Georgia, Athens, GA 30602 USA.

<sup>†</sup>Electronic Supplementary Information (ESI) available: Experimental details, additional structural and spectral characterization of mediators and QDs, quantum efficiency measurements. See DOI: 10.1039/x0xx00000x

electron shuttle in several ways. The position of the pyridyl methyl substituent affects both the electronic structure of the mediator and the sterics of its interaction with a nanocrystalline semiconductor surface. The carbon chain linking the two pyridyl nitrogens introduces a twist in the torsion angle of the two rings that depends on the chain length. Evidence of the twist along the bipyridine core is clear in the X-ray structures (Fig. 1) and in NMR spectra (Fig. S1, ESI<sup>†</sup>) of the mediators and is consistent with previous reports.<sup>14</sup> Representative X-ray structures for DQ52 and DQ03 are presented in Fig. 1 (detailed structural information for all mediators given in Tables S1, S2, ESI<sup>†</sup>). The average torsional twist between pyridyl rings was  $\sim 19^\circ$  for those mediators with a two-carbon chain linker and  $\sim 53^\circ$  for those with a three-carbon chain linker. The torsional twist also causes important changes to the electronic structure of the mediators. These changes are reflected in the reduction potential, which becomes more negative as the torsional twist increases. Previous molecular orbital (MO) calculations for mediators with 2C and 3C linkers showed that increasing the torsional twist disrupts the conjugated system and shifts the LUMO to a higher energy.<sup>14</sup> The effect on mediator electronic structure is also reflected in the UV-Vis absorbance spectra of the di-cation and mono-cation forms (Fig. 2 and Fig. S2, ESI<sup>†</sup>). The  $\pi \rightarrow \pi^*$  transition of the di-cation is observed to shift to higher energy with increasing torsional twist.<sup>15</sup> This blue shift is related to the change in  $\Delta E$  between HOMO and LUMO with twist angle. MO calculations indicate that  $\Delta E$  increases due to the increase in the LUMO energy, consistent with our observation of more negative reduction potentials in the cyclic voltammetry data (Fig. S3).<sup>14</sup> In contrast, the  $\pi \rightarrow \pi^*$  transition of the reduced mediators is observed to shift to lower energy with increasing linker length (Fig. 2A). This red-shift has been attributed previously to a more planar structure for the radical species.<sup>14, 15</sup> The decrease in torsional twist associated with radical cation formation allows for a greater degree of orbital overlap between the bipyridinium rings, leading to the lower energy transition. Slower ET rates are observed as the twist angle is increased, due to an increase in reorganization energy required to reach the planar structure of the reduced state.<sup>16</sup> Electronic structure calculations of DQ03 also support a change in geometry of the mediator from the twisted form to a more planar configuration upon reduction.<sup>14</sup>

The first step in the electron shuttle process is ET from the conduction band (CB) of the excited CdSe QD to the mediator. We performed steady-state photo-illumination experiments to determine the quantum efficiency for reduction of the mediator ( $QE_{\text{rad}}$ ) as shown in Fig. 2. Illumination of the CdSe QD with blue light (405 nm) produces an exciton state, which the mediator quenches by extracting an electron from the CB, generating a population of the reduced mediator radical cation (mediator<sup>•+</sup>). The hole left in the VB of the CdSe QD is scavenged by the sacrificial electron donor (SED), mercaptopropionic acid (MPA). This ET event ( $k_{\text{CS}}$ ) is depicted schematically in Fig. 2D with the relative LUMO energies of the mediators. Absorbance spectra of the radical cations are shown in Fig. 2A. The absorbance feature at either 450 nm or 510 nm was monitored for each mediator depending on whether the spectrum belonged to a 2C or 3C linked molecule, respectively. The concentration

of the reduced mediator versus illumination time (Fig. 2B) is determined from the measured extinction coefficient of each radical species.  $QE_{\text{rad}}$  was determined by dividing the moles of radical generated by the moles of photons absorbed by the

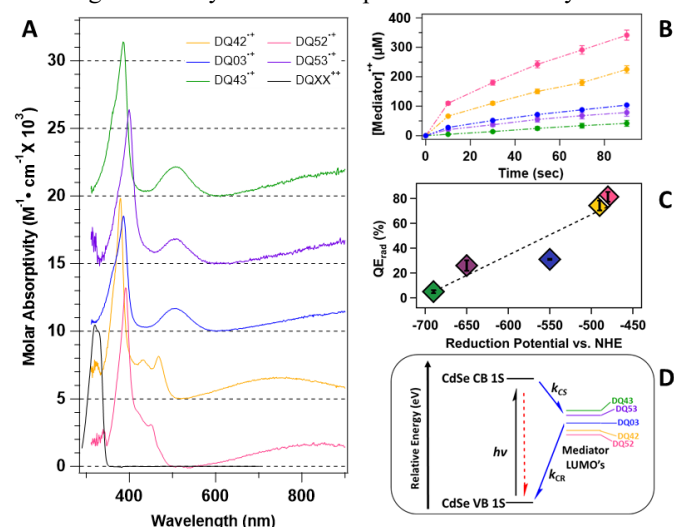


Fig. 2. Steady-state photoreduction experiments with CdSe QDs and mediators. (A) UV-vis extinction spectra for reduced mediators compared to oxidized DQ03<sup>2+</sup>; spectra are offset for clarity. (B) Kinetics of photoreduction of mediator, quantified by monitoring absorbance at 450 or 510 nm for 2C or 3C linked radical species, respectively. (C) Dependence of quantum efficiency for reduction of mediators on reduction potential. (D) Schematic depicting the ET processes and energies of CdSe QD conduction band (CB) and valence band (VB) relative to the mediator LUMO energies.

solution and correcting for reflection from the front face of the cuvette. We calculate the quantum yield from the first 10 seconds of illumination, before the concentration of mediator<sup>•+</sup> builds up, thus minimizing contributions from back ET ( $k_{\text{CR}}$ ) and other parasitic processes that lead to mediator degradation (full details of the calculation are presented in the ESI<sup>†</sup>).<sup>7</sup>

The rate of formation of mediator<sup>•+</sup> is constant in the first 10 seconds but begins to decline after this initial phase (Fig. 2B). The decrease in the rate of formation of mediator<sup>•+</sup> is attributed to consumption of the mediator di-cation and to an increased rate of charge recombination at high concentrations of mediator<sup>•+</sup>. At longer times, the rate of mediator reduction and charge recombination are balanced and the system reaches a steady state. The initial rates of mediator<sup>•+</sup> formation and steady state concentrations vary with the reduction potential of the mediator (Fig. 2B), with the 2C linker mediators having significantly faster initial rates and reaching larger steady state populations than the 3C linker ones. It is clear the 2C linker molecules, DQ42 and DQ52, have the highest net  $QE_{\text{rad}}$  (Fig. 2C). The differences in  $QE_{\text{rad}}$  is best explained by considering the faster  $k_{\text{CS}}$  and the slower  $k_{\text{CR}}$  observed for the 2C linked mediators relative to the 3C linked ones. The result of a faster  $k_{\text{CS}}$  and slower  $k_{\text{CR}}$  is a net higher  $QE_{\text{rad}}$  and therefore larger steady state populations of reduced mediator, as strongly suggested by the steady-state data.

The differences in ET rates and net  $QE_{\text{rad}}$  for this series of mediators can be understood in terms of the reduction potentials, which influence both the forward and reverse ET reactions.<sup>17</sup> Fig. 2C shows the dependence of the net  $QE_{\text{rad}}$  on the reduction potential of the mediator. The energetics of this process are illustrated in Fig. 2D, where the relative energy levels were

determined from the reduction potentials of the mediators and the band edge of the CdSe QDs. The 2C linker mediators with the more positive redox potentials (lower energy LUMO's) have a larger downhill driving force for forward ET and a smaller driving force for back ET, resulting in larger  $k_{CS}$  and smaller  $k_{CR}$  (normal Marcus regime). The net result is a long-lived charge separated state and high  $QE_{rad}$ . The situation is more complex for the 3C linker mediators, since their more negative reduction potential yields a driving force for back ET in the Marcus inverted regime, resulting in a decrease in  $k_{CR}$ .

It is also likely that the rate of ET from the QD to the mediator and the net  $QE_{rad}$  are affected by the differences in reorganization energy for forward and reverse ET across this series. The reorganization energy is influenced by the torsional twist between the pyridyl rings of the mediators, since the reduced mediator adopts a more planar structure.<sup>16</sup> Thus, the reorganization energy for the more highly twisted 3C linker molecules is expected to be larger than that for the 2C linker molecules. This increased reorganization energy is expected to slow down the ET to the 3C linker molecules relative to the 2C linker ones, leading to less efficient charge separation. For example, the net  $QE_{rad}$  drops dramatically from 74% to 31% between DQ42 and DQ03 as the twist in the bipyridyl core is increased from  $\sim 22^\circ$  to  $\sim 55^\circ$ . Further study would be required to assess the relative contributions of reorganization energy and driving force to the difference in net  $QE_{rad}$ , but both are likely important.

The next step in the electron shuttle process is ET from mediator<sup>+</sup> to the hydrogenase and turnover of the enzyme to produce hydrogen. We measured hydrogen production efficiency for a hybrid system consisting of CdSe QDs, mediator and the [NiFe] SHI from *Pyrococcus furiosus* (*Pf*) as the hydrogen production catalyst. *Pf*SHI is a robust catalyst, having high thermal stability and oxygen tolerance.<sup>18</sup> It also has a high turnover rate at neutral pH ( $100\text{ s}^{-1}$  at room temperature) and operates near the thermodynamic potential of the hydrogen couple. Hydrogen production assays were carried out at pH 7.1 under conditions analogous to those used in the mediator photoreduction experiments. Fig. 3A shows the time dependent yields of light driven hydrogen production for each of the mediators. Furthermore, addition of a mediator to this hybrid system significantly improves overall quantum yield for hydrogen production compared to related systems that rely on direct ET from the NCS material to the hydrogenase. The net production of  $H_2$  and the corrected  $QE_{hyd}$  for each mediator are summarized in Table 1.

Trends in the  $QE_{hyd}$  indicate a strong correlation between the reduction potential of the mediator and amount of  $H_2$  produced as shown in Fig. 3B. Previously, we investigated the effect of the mediator reduction potential on the efficiency of a related hybrid CdSe/CdS nanorod-hydrogenase photocatalytic system.<sup>7</sup> We compared two mediators, methyl viologen ( $MV^{2+}$ ,  $E_0 = -446\text{ mV}$  vs. NHE) and DQ03 (or  $PDQ^{2+}$ ,  $E_0 = -550\text{ mV}$  vs. NHE) and found significantly better performance with DQ03, due to its greater driving force for ET to the surface exposed FeS cluster of SHI. With DQ03 and nanorods, we achieved the highest reported quantum yield for hydrogen production with such

**Table 1** Steady State Hydrogen Production (at 5000 sec)

Mediator	Solution Potential (mV) <sup>a</sup>	Moles $H_2$	$QE_{corr}$ (%)
DQ52	-375	$4.1 \times 10^{-7}$	4.7
DQ42	-385	$8.1 \times 10^{-7}$	7.8
DQ03	-410	$2.7 \times 10^{-6}$	14.8
DQ53	-425	$3.7 \times 10^{-6}$	16.8
DQ43	-495	$2.6 \times 10^{-6}$	11.5

<sup>a</sup>Versus SHE; determined from the Nernst equation:  $\Delta E = \Delta E^\circ - \frac{RT}{F} \ln \frac{[Med^{+}]}{[Med^{2+}]}$

hybrid photocatalytic systems.<sup>7</sup> The current results are consistent with the previous ones, showing greater overall efficiency of hydrogen production with increased driving force for electron transfer from the reduced mediator to the enzyme. The highest observed quantum efficiency for  $H_2$  production is modest ( $QE_{hyd} = 16.8\%$ ) compared to previous results with nanorods ( $QE_{hyd} = 52\%$  for similar conditions). This difference in efficiency is primarily due to the NCS photosensitizer, since the nanorod structure has a significantly longer exciton lifetime than the QD, leading to a greater efficiency of the charge separation process. Nevertheless, the yields for the three highest performing mediators in the present work are significantly higher than what has been observed previously with CdSe QD's.<sup>19</sup>

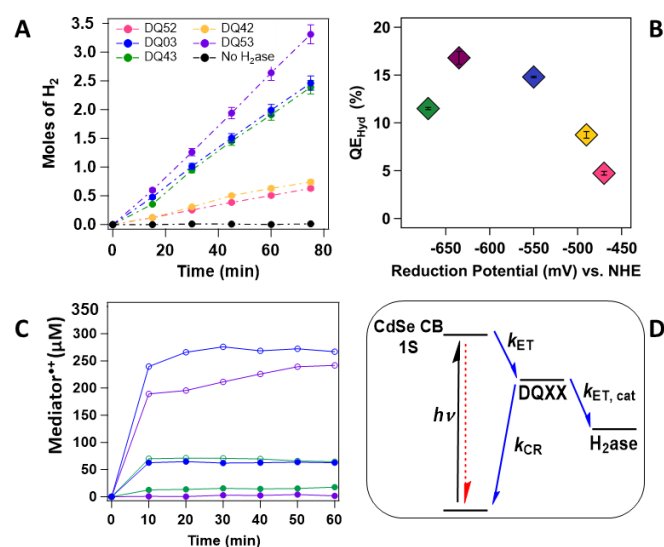


**Fig. 3.** Steady-State  $H_2$  Production. (A)  $H_2$  production as a function of laser illumination time: DQ53 (purple), DQ43 (green), DQ03 (blue), DQ42 (yellow), DQ52 (pink), no mediator present (black). (B) Correlation of  $H_2$  generation efficiency ( $QE_{hyd}$ ) with reduction potential. (C) Production of reduced mediator versus illumination time with  $H_2ase$  (closed circles) and without  $H_2ase$  (open circles). (D) Energy diagram of ET steps.

The correlation of photocatalytic hydrogen production efficiency with reduction potential of the mediator is inverse to the trend observed for the steady-state mediator photoreduction experiments. This observation highlights the complex interplay between the net yield of hydrogen production and the rates of charge separation, charge recombination and ET to the enzyme, as shown in the scheme in Fig. 3D. Optimum hydrogen production requires a balance between driving force for the two forward ET processes; decreasing the mediator LUMO energy

decreases the driving force for ET to the catalyst ( $k_{ET}$ ), but at the same time increases the driving force for reduction of the mediator ( $k_{CS}$ ). Thus, while the mediators that are easier to reduce (lower LUMO energies) exhibit a higher quantum efficiency for photoreduction by the QDs, they are less effective at reducing the enzyme and producing hydrogen. In contrast, charge recombination becomes more rapid as the LUMO energy is increased, which lowers the net yield of photoreduction in the absence of enzyme. In the presence of enzyme, however, ET to the enzyme is competitive with charge recombination and thus efficient hydrogen production can be achieved.

Further insight on the optimum parameters for hydrogen production is provided by considering the solution potential achieved under illumination at steady state. Fig. 3C shows the production of reduced mediator as a function of illumination time for DQ03, DQ43, and DQ53 mediators with and without hydrogenase present. The reduced mediator concentration increases initially then reaches a constant value; a lower steady state population is reached in the presence of hydrogenase, due to ET to the enzyme. It is clear that in all cases the system reaches steady state (constant mediator<sup>+</sup> concentration) within an hour. Therefore, we determined the steady state solution potential by measuring the concentration of reduced mediator from the radical absorbance after 5000 sec of illumination. The Nernst equation was then used to calculate the solution potential from the relative concentration of mediator<sup>+</sup>/mediator<sup>+</sup>, yielding the values shown in Table 1. For comparison, at pH 7.1 the hydrogen couple is at -419 mV. The most efficient mediators DQ03, DQ53 and DQ43 reach steady state solution potentials near or more negative than the hydrogen couple. In contrast, with DQ42 and DQ52 the steady state solution potentials are significantly more positive than the hydrogen couple and therefore proton reduction is not as favorable for the 2C linker mediators.

The hydrogen production efficiency peaks with DQ53 even though it does not have the most negative reduction potential. DQ53<sup>+</sup> concentration levels close to those observed for DQ03<sup>+</sup> are achieved when the solution contains solely dots and mediator (Fig. 3C). When the enzyme is present, however, steady state illumination produces a barely observable population of DQ53<sup>+</sup>, indicating that its consumption by the enzyme is rapid. Based on this evidence, it is likely that the conditions are not fully optimized for hydrogen production in the case of DQ53. Utilization of a photosensitizer with a longer-lived exciton, such as a nanorod, would increase the  $QE_{hyd}$  produced with DQ53, since it would increase  $QE_{rad}$ . The lower  $QE_{hyd}$  observed with DQ43 is in part due to inefficient ET to the enzyme despite its more negative reduction potential, resulting in a higher steady state population of mediator<sup>+</sup> compared to DQ53 (Fig. 3C). Slower ET to the enzyme for DQ43 might be an indication of entrance into the Marcus inverted regime, wherein having an increased driving force slows ET to the enzyme, resulting in a lower than expected  $QE_{hyd}$ .

In this report, we have optimized the hydrogen production efficiency of a hybrid photocatalytic system consisting of a nanocrystalline semiconductor (CdSe QD) photosensitizer and a hydrogenase enzyme (*Pf*SHI). The performance was optimized by tuning the structure and reduction potential of the redox

mediator that serves as an electron shuttle between the QD and enzyme. Optimum performance requires a careful balance among the rates of charge separation, ET to the enzyme and charge recombination, which can be achieved by tuning the energy of the mediator LUMO. The versatility of this modular system makes it attractive for additional studies with other photosensitizer materials and with other biological or manmade catalysts for PCET processes such as CO<sub>2</sub> reduction.

The authors thank Dr. John Bacsá for help with X-ray crystal structure determination. Funding for this work was provided by the National Science Foundation (grants CHE1807865 and DMR1808288 to RBD) and by the Division of Chemical Sciences, Geosciences and Biosciences, Office of Basic Energy Sciences of the U.S. Department of Energy (grant DE-FG05-95ER20175 to MWA).

## Conflicts of interest

There are no conflicts to declare.

## Notes and references

- 1 K. A. Brown, D. F. Harris, M. B. Wilker, A. Rasmussen, N. Khadka, H. Hamby, S. Keable, G. Dukovic, J. W. Peters, L. C. Seefeldt and P. W. King, *Science*, 2016, **352**, 448-450.
- 2 M. Đokić and H. S. Soo, *Chem. Commun.*, 2018, **54**, 6554-6572.
- 3 B. L. Greene, C. A. Joseph, M. J. Maroney and R. B. Dyer, *J. Am. Chem. Soc.*, 2012, **134**, 11108-11111.
- 4 K. A. Brown, M. B. Wilker, M. Boehm, H. Hamby, G. Dukovic and P. W. King, *ACS Catalysis*, 2016, **6**, 2201-2204.
- 5 K. A. Brown, S. Dayal, X. Ai, G. Rumbles and P. W. King, *J. Am. Chem. Soc.*, 2010, **132**, 9672-9680.
- 6 T. W. Woolerton, S. Sheard, Y. S. Chaudhary and F. A. Armstrong, *Energy Environ. Sci.*, 2012, **5**, 7470-7490.
- 7 B. Chica, C.-H. Wu, Y. Liu, M. W. W. Adams, T. Lian and R. B. Dyer, *Energy Environ. Sci.*, 2017, **10**, 2245-2255.
- 8 M. S. Kodaimati, K. P. McClelland, C. He, S. Lian, Y. Jiang, Z. Zhang and E. A. Weiss, *Inorg. Chem.*, 2018, **57**, 3659-3670.
- 9 H. Zhu, N. Song, H. Lv, C. L. Hill and T. Lian, *J. Am. Chem. Soc.*, 2012, **134**, 11701-11708.
- 10 E. A. Weiss, *ACS Energy Lett.*, 2017, **2**, 1005-1013.
- 11 M. D. Peterson, S. C. Jensen, D. J. Weinberg and E. A. Weiss, *ACS Nano*, 2014, **8**, 2826-2837.
- 12 A. J. Morris-Cohen, M. D. Peterson, M. T. Frederick, J. M. Kamm and E. A. Weiss, *J. Phys. Chem. Lett.*, 2012, **3**, 2840-2844.
- 13 J. Chen, K. Wu, B. Rudshsteyn, Y. Jia, W. Ding, Z.-X. Xie, V. S. Batista and T. Lian, *J. Am. Chem. Soc.*, 2016, **138**, 884-892.
- 14 S. H. R. Brienne, P. D. W. Boyd, P. Schwerdtfeger, G. A. Bowmaker and R. P. Cooney, *J. Mol. Struct.*, 1995, **356**, 81-94.
- 15 S. Yasui, K. Itoh, A. Ohno and N. Tokitoh, *Org. Biomol. Chem.*, 2006, **4**, 2928-2931.
- 16 S. Yasui, K. Itoh, A. Ohno and N. Tokitoh, *Org. Biomol. Chem.*, 2006, **4**, 2928-2931.
- 17 H. Zhu, Y. Yang, K. Wu and T. Lian, *Annu. Rev. Phys. Chem.*, 2016, **67**, 259-281.
- 18 B. L. Greene, C.-H. Wu, P. M. McTernan, M. W. W. Adams and R. B. Dyer, *J. Am. Chem. Soc.*, 2015, **137**, 4558-4566.
- 19 S. Kundu and A. Patra, *Chem. Rev.*, 2017, **117**, 712-757.